Proceedings of the 8th WSEAS International Conference on APPLIED MATHEMATICS, Tenerife, Spain, December 16-18, 2005 (pp19-24)

Radiation in Numerical Compactons from Finite Element Methods

JULIO GARRALÓN[†] FRANCISCO RUS[†] FRANCISCO R. VILLATORO[§]

Dept. Lenguajes y Ciencias de la Computación[†]
E.T.S. Ingenieros de Telecomunicación, Universidad de Málaga
Campus de Teatinos, s/n, 29071, Málaga
SPAIN

Dept. Lenguajes y Ciencias de la Computación[§]
E.T.S. Ingenieros Industriales, Universidad de Málaga
Campus El Ejido, s/n, 29013, Málaga
SPAIN

jgr,rusman,villa@lcc.uma.es http://www.lcc.uma.es/

Abstract: - The numerical simulation of the propagation of nonlinear waves may present numerically-induced radiation. Compactons, solitary waves with compact support, are no exception. The numerical radiation generated by compactons of the Rosenau-Hyman $K(2,2)$ equation calculated by means of a fourth-order finite element method is illustrated. Small-amplitude forward and backward radiation are shown in the simulations, both having self-similar envelope profiles and high frequency carriers. The amplitude and velocity of the envelope of both radiations are determined.

Key-Words: - Compactons, Numerical radiation, Finite element methods, Self-similarity

1 Introduction

The numerical simulation of the propagation of nonlinear waves presents several numerically induced phenomena, such as spurious radiation, artificial dissipation, or errors in group velocity. The numerical analysis of compactons [1], traveling wave solutions with compact support resulting from the balance of both nonlinearity and nonlinear dispersion, are not free of these spurious phenomena. In fact, the numerical solution of compacton equations is a very challenging problem presenting several numerical difficulties which have not been currently explained [2, 3].

For the numerical simulation of compactons, pseudospectral, finite element, finite difference and particle methods have been used in space. Pseudospectral methods require the addition of artificial dissipation (hyperviscosity) using high-pass filters [1, 4] in order to obtain stable results. The main drawback of current (filtered) pseudospectral methods is the inability to show high-frequency phenomena [2, 5]. Particle methods based on the dispersive-velocity method have been proposed to cope with these features [4], but their preservation of the positivity of the solutions is another clear disadvantage. In finite element methods both a Petrov-Galerkin method using the product approximation developed by Sanz-Serna and Christie [2], and a standard method based on piecewise polynomials discontinuous at the element interfaces [6] have been used. Second-order finite difference methods [7], high-order Padé methods [5], and the method of lines with adaptive mesh refinement [3] have also been applied with success. Both finite difference and finite element methods require artificial dissipation to simulate the generation of high-frequency phenomena during compacton interactions, which is usually incorporated by a linear fourth-order derivative term.

The main drawback in the numerical simulation of compacton propagation without high-frequency filtering is the appearance of spurious radiation, even in one-compacton solutions. Since this radiation is usually of very small amplitude, in fact, more than six orders of magni-

tude smaller than the compacton amplitude in current simulations, it has not been previously noticed in the literature. In this paper, for the first time, this spurious radiation is illustrated and their main properties determined. In order to focus our analysis, only the numerical solution of the Rosenau-Hyman $K(2,2)$ compacton equation is studied. Moreover, extensive numerical studies [2, 3, 5, 6, 7] shows that the best method for the solution of this equation is the fourth-order Petrov-Galerkin finite element method developed by de Frutos, López-Marcos and Sanz-Serna [2]. In this paper we further focus our attention in the spurious radiation generated by this method. Other methods yield similar results to be reported elsewhere.

The contents of this paper are as follows. Next Section shows the mathematical expression of the compacton solution of the Rosenau-Hyman $K(n,n)$. Section 3 shows the derivation, truncation error terms and linear stability of the finite element method used in our simulations. Section 4 presents our results on both the forward and the backward numerically-induced radiation wavepackets generated during the propagation of one-compacton solutions. Finally, the last section is devoted to some conclusions.

2 Compacton solutions

Compactons were first found as solutions of the (focusing) $K(n,n)$ compacton equation by Rosenau and Hyman [1], which is given by

$$u_t + (u^n)_x + (u^n)_{xxx} = 0, \qquad 1 < n \leq 3, \quad (1)$$

where $u(x,t)$ is the wave amplitude, x is the spatial coordinate, t is time, and the subindexes indicate differentiation. Equation (1) has four invariants $I_i = \int \phi_i(u)\,dx$, where $\phi_1 = u$, $\phi_2 = u^{n+1}$, $\phi_3 = u\,\cos(x)$, and $\phi_4 = u\,\sin(x)$.

Compacton solutions of Eq. (1), for $n \notin \{-1, 0, 1\}$, can be written as [9]

$$u_c(x,t) = \begin{cases} \left(\alpha\,\cos^2\left(\beta\,(x - x_0 - c\,t)\right)\right)^{\mu}, \\ \qquad\qquad |x - x_0 - c\,t| \leq \dfrac{\pi}{2\,\beta}, \\ 0, \qquad\qquad \text{otherwise}, \end{cases}$$

where c is the compacton velocity, x_0 the position of its maximum at $t = 0$, and

$$\alpha = \frac{2\,c\,n}{n+1}, \quad \beta = \frac{n-1}{2\,n}, \quad \mu = \frac{1}{(n-1)}.$$

Compacton solutions are classical solutions only for $1 < n \leq 3$, otherwise they are weak solutions.

3 Finite element method

Extensive numerical studies developed by both de Frutos, López-Marcos and Sanz-Serna [2] and Ismail and Taha [7], among others, shows that the best method for the solution of Eq. (1) is a Petrov-Galerkin finite element method previously developed by Sanz-Serna and Christie [8] for the Korteweg-de Vries equation.

In Petrov-Galerkin methods trial and test function spaces are not the same. Here, C^0 continuous piecewise linear interpolants and C^2 continuous Schoenberg cubic B-splines are used respectively as trial and test functions. For the nonlinear terms, the product approximation is applied. The resulting weak formulation for Eq. (1) is as follows: Find a function

$$u(x,t) = \sum_{i=0}^{N} U_i(t)\,\phi_i(x),$$

such that

$$\langle U_t, \psi_j\rangle + \langle (U^n)_x, \psi_j\rangle + \langle (U^n)_x, (\psi_j)_{xx}\rangle = 0, \quad (2)$$

for all $\psi_j(x)$, $j = 0, 1, \ldots, N$, where a uniform mesh is used, $x_i = x_0 + i\,\Delta x$, the inner product is

$$\langle f, g\rangle = \int_{x_0}^{x_N} f(x)\,g(x)\,dx,$$

$U_i(t) = U(x_i,t) \approx u(x_i,t)$, $\phi_i(x)$ are the usual piecewise linear hat functions associated with the node x_i ($\phi_i(x_j) = \delta_{ij}$, the Kronecker delta), which can be written as

$$\phi_i(x) = \begin{cases} \dfrac{x - x_{i-1}}{\Delta x}, & x \in [x_{i-1}, x_i], \\ \dfrac{x_{i+1} - x}{\Delta x}, & x \in [x_i, x_{i+1}], \\ 0, & \text{elsewhere}, \end{cases}$$

and $\psi_j(x)$ are cubic B-splines defined in a $4\,\Delta x$

interval, given by

$$\psi_i(x) = \begin{cases} \dfrac{(x-x_{i-2})^3}{\Delta x^3}, & x \in [x_{i-2}, x_{i-1}], \\ 1 + 3\,\dfrac{x-x_{i-1}}{\Delta x} + 3\,\dfrac{(x-x_{i-1})^2}{\Delta x^2} \\ \quad -3\,\dfrac{(x-x_{i-1})^3}{\Delta x^3}, & x \in [x_{i-1}, x_i], \\ 1 + 3\,\dfrac{x_{i+1}-x}{\Delta x} + 3\,\dfrac{(x_{i+1}-x)^2}{\Delta x^2} \\ \quad -3\,\dfrac{(x_{i+1}-x)^3}{\Delta x^3}, & x \in [x_i, x_{i+1}], \\ \dfrac{(x_{i+2}-x)^3}{\Delta x^3}, & x \in [x_{i+1}, x_{i+2}], \\ 0, & \text{elsewhere}, \end{cases}$$

which are C^2 continuous as required by Eq. (2).

Tedious evaluation of the inner products in Eq. (2) yields the following system of ordinary differential equations

$$\mathcal{A}(\mathrm{E})\,\frac{dU_j}{dt} + \mathcal{B}(\mathrm{E})\,(U_j)^n + \mathcal{C}(\mathrm{E})\,(U_j)^n = 0, \quad (3)$$

where E is the shift operator, i.e., $\mathrm{E}\,U_j = U_{j+1}$, and

$$\mathcal{A}(\mathrm{E}) = \frac{\mathrm{E}^{-2} + 26\,\mathrm{E}^{-1} + 66 + 26\,\mathrm{E}^{1} + \mathrm{E}^{2}}{120},$$

$$\mathcal{B}(\mathrm{E}) = \frac{-\mathrm{E}^{-2} - 10\,\mathrm{E}^{-1} + 10\,\mathrm{E}^{1} + \mathrm{E}^{2}}{24\,\Delta x},$$

$$\mathcal{C}(\mathrm{E}) = \frac{-\mathrm{E}^{-2} + 2\,\mathrm{E}^{-1} - 2\,\mathrm{E}^{1} + \mathrm{E}^{2}}{2\,\Delta x^3}.$$

The method of lines given by Eq. (3) is fourth-order accurate for regular enough solutions ($U_j(t) \in \mathrm{C}^7$), since its truncation error terms are given by

$$U_t + (U^n)_x + (U^n)_{xxx} = \frac{\Delta x^4}{240}\,\frac{\partial^7 U}{\partial x^7} + O\big(\Delta x^6\big)\,.$$

However, in multi-compacton solutions of the $K(n,n)$ equation, even for smooth initial data, shocks (or nonsmooth solutions) are developed reducing the effective order of accuracy locally around the shocks and introducing numerical instabilities which evolve to the blow-up of the solution [2, 5]. In order to avoid these instabilities, artificial viscosity must be introduced into the nondissipative method given by Eq. (3). Here, the term $\epsilon\,\partial^4 u/\partial x^4$, with ϵ small enough, is introduced into the left-hand side of Eq. (1). This term is numerically discretized by means of a second-order accurate five-point difference formula, given by

$$\epsilon\,\mathcal{D}(\mathrm{E})\,U_j = \epsilon\,\frac{\mathrm{E}^{-2} - 4\,\mathrm{E}^{-1} + 6 - 4\,\mathrm{E}^{1} + \mathrm{E}^{2}}{\Delta x^4}\,U_j,$$

which is added to the left-hand side of Eq. (3).

The second-order implicit midpoint rule is used for the integration in time of Eq. (3), yielding

$$\mathcal{A}(\mathrm{E})\,\frac{U_j^{m+1} - U_j^m}{\Delta t} + (\mathcal{B}(\mathrm{E}) + \mathcal{C}(\mathrm{E}))\,\left(\frac{U_j^{m+1} + U_j^m}{2}\right)^n + \epsilon\,\mathcal{D}(\mathrm{E})\,\left(\frac{U_j^{m+1} + U_j^m}{2}\right) = 0, \quad (4)$$

where $U_j^m \approx u(x_j, m\,\Delta t)$. The resulting nonlinear system of algebraic equations is solved by means of Newton's method. The linear stability analysis by the von Neumann method for Eq. (4) with $\epsilon = 0$, after linearization by taking $(U_j^m)^n = \|W\|\,U_j^m$, with $\|W\| = n\,(\|u\|_\infty)^{n-1}$, and substituting $U_j^m = r^m\,\exp(\mathrm{i}\,j\,\theta)$, $\mathrm{i} = \sqrt{-1}$, yields the amplification factor

$$|r| = \frac{|A - \mathrm{i}\,\|W\|\,\sin\theta\,B|}{|A + \mathrm{i}\,\|W\|\,\sin\theta\,B|},$$

where

$$A = 33 + 26\,\cos\theta + \cos 2\theta,$$

$$B = \frac{5}{2}\,\frac{\Delta t}{\Delta x}\,(5 + \cos\theta) + 30\,\frac{\Delta t}{\Delta x^3}\,(\cos\theta - 1).$$

Therefore, $|r| = 1$ and Eq. (4) for $\epsilon = 0$ is nondissipative and (linearly) unconditionally stable. In practice, for nonsmooth solutions these schemes may blow up if artificial viscosity (small but nonnull ϵ) is not introduced.

The finite element method developed here preserves exactly the first invariant of the $K(n,n)$ equation (for $\epsilon = 0$), since by summing in space it may be easily shown that $\sum_m u_m^n = \sum_m u_m^0$. However, the other three invariants are not exactly preserved, but instead only well preserved, as shown in Figure 1. The error in the first invariant shown in Figure 1 (top plot) is not exactly

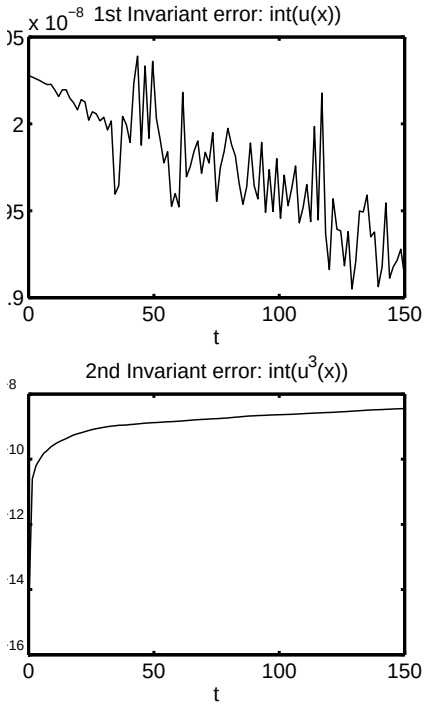

Figure 1: The error between the analytical value and the numerical one calculated by the trapezoidal quadrature rule for the first (top plot) and second (bottom plot) invariants during the propagation of the 1-compacton solution of the $K(2,2)$ equation.

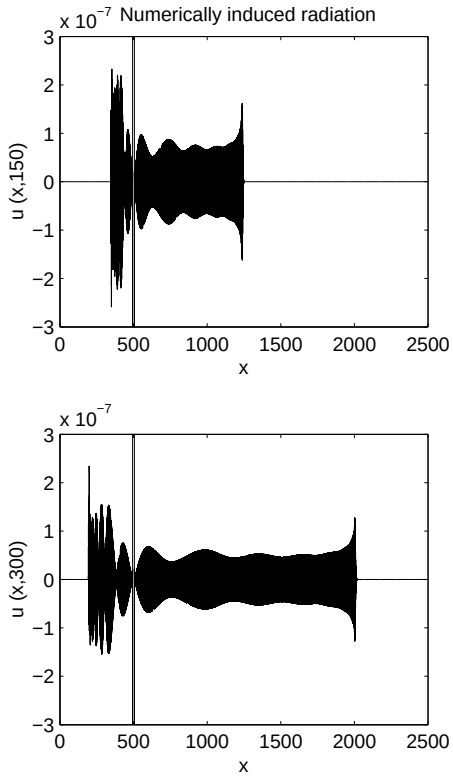

Figure 2: Radiation generated at both sides of a compacton propagating with $c = 1$ at two instants of time, $t = 100$ (top plot) and $t = 250$ (bottom plot).

null, as theoretically predicted, because of the errors introduced by the Newton iteration which has been stopped when the relative error in the solution is smaller than 10^{-10}. Since the error in the second invariant is very similar in magnitude to that of the first one, so this invariant is also very well preserved.

4 Presentation of results

Extensive numerical experiments with the finite element method developed in the previous Section have verified their good accuracy and conservation properties for both $\epsilon = 0$ and, when required, small enough properly chosen ϵ. The main result of this paper is the discovery, for $\epsilon = 0$, of numerically induced radiation resulting from the propagation of the numerical compacton. Both backward- and forward-propagating wavepackets have been found. In order to focus the scope of the paper, only results for the $K(2,2)$ equation are presented.

Figure 2 shows a zoom in of compacton with $c = 1$ where a moving frame of reference $X = x - c\,t$ is used in order to stop the compacton and to highlight the relative velocity of the wavepackets of radiation generated during its propagation. As clearly shown in both plots, two wavepackets of radiation propagate from the compacton, here referred to as forward and backward radiation corresponding to that with a group velocity larger and smaller, respectively, than the compacton velocity. The amplitude of both wavepackets is very small compared with that of the compacton, hence they may be considered negligible in many practical simulations.

The more interesting and noticeable property of both backward and forward compacton radiation is their self-similarity. Figures 3 and 4 clearly show this property presenting, respectively, plots of forward and backward radiation at two instants of time stretching the horizontal axis in order to highlight the self-similarity of the wavepackets. Similar results have been obtained for other instants of time and for compactons with other velocities.

Backward and forward numerically-induced radiation are characterized by the evolution of their

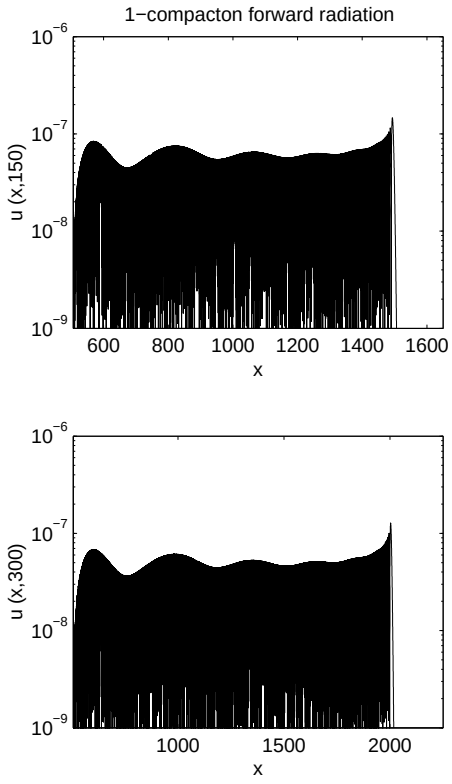

Figure 3: Forward radiation generated during a compacton propagation with $c = 1$ at two instants of time, $t = 200$ (top plot) and $t = 300$ (bottom plot), highlighting their self-similarity.

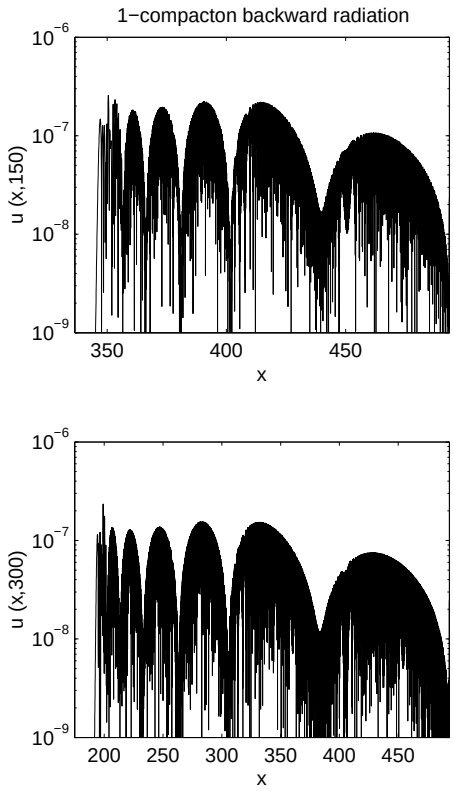

Figure 4: Backward radiation generated during a compacton propagation with $c = 1$ at two instants of time, $t = 200$ (top plot) and $t = 300$ (bottom plot), highlighting their self-similarity.

amplitude and group velocity relative to that of the compacton, shown in Figure 5. The amplitude of the radiation may be calculated locally by searching the first maximum of the radiation from the outside of the wavepacket. This maximum changes a little in the first steps of time but yield a very smooth curve as time progresses, as shown in the top plot of Figure 5, which also illustrates their nearly exponential diminution in time of both the backward and forward radiation. Similar results have been obtained for other compacton and/or mesh parameters.

The velocity of the front of the wavepackets of both forward (c_F) and backward (c_B) radiation relative to the velocity of the compacton can be easily obtained from plots of the position of the "first" peak of the wavepacket, that used to calculate its amplitude. Figure 5 (bottom plot) shows the position of this radiation front for both the backward and the forward wavepackets, showing that the velocity of this front is practically constant during propagation and may be calculated by linear regression of the data of their positions.

Table 1: Velocity of the front of both the backward and forward radiation for a compacton with velocity $c = 1$ in numerical simulations with $\Delta t = 0.05$ for several values of Δx with $x \in [0, 2500]$ and $t \in [0, 300]$.

Δx	0.2	0.1	0.05	0.025	0.0125
c_F	5.063	5.034	5.022	5.013	5.004
$-c_B$	1.004	1.005	1.004	0.997	1.000

Table 1 shows the results of such a procedure as a function of the spatial grid size Δx and fixed Δt. This table shows that both the forward (c_F) and backward (c_B) group velocities are practically constant, equating 5 and -1, approximately. A similar table for the variation as a function Δt shows similar trends. Further results, omitted here for brevity, indicate that c_F and c_B depends mainly on the compacton velocity (or amplitude), being nearly independent of the parameters of the numerical method.

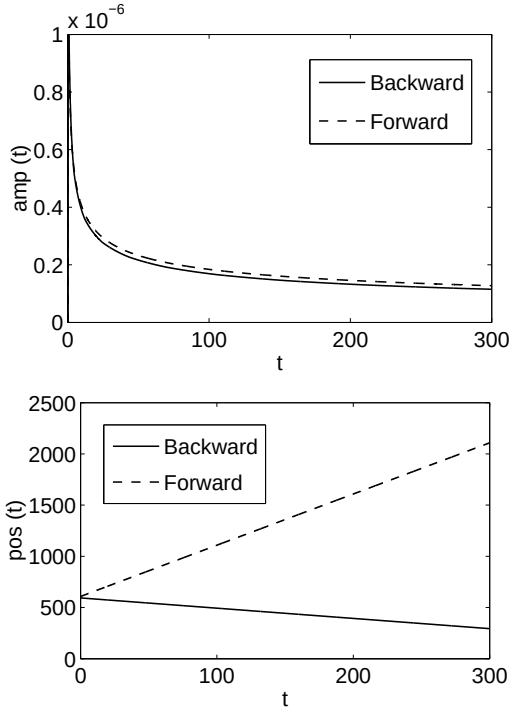

Figure 5: Amplitude (top plot) and front velocity (bottom plot) of both forward (dashed line) and backward (continuous line) radiations as a function of time.

5 Conclusions

The propagation of compactons of the Rosenau-Hyman equation has been studied by means of a fourth-order accurate Petrov-Galerkin finite element method. For the first time, numerically induced radiation in the propagation of numerical compactons has been reported. Both backward and forward radiation is found and their parameters have been determined using a moving frame of reference stopping the compacton. Both kind of radiation were shown to be self-similar, showing a nearly exponentially decreasing amplitude and nearly constant velocity, strongly depending on the parameters of the compacton but only slightly depending on the parameters of the numerical method.

Further research on the characterization of the radiation of numerical compactons based on other numerical methods, in fact, finite difference, Padé methods and other finite element techniques is in progress. The quantification of the self-similarity by means of the correlation function and the determination of their scaling parameters are also in progress. Finally, the behaviour of the spurious radiation under high-frequency filtering also devotes some attention.

Acknowledgements: J. G. and F. R. were partially supported by the CICYT grant TIC2002-04309-C02-02 (Spain), and F. R. V. by the DGICT under grant FIS2005-03191 (Spain).

References:

[1] P. Rosenau and J. M. Hyman, Compactons: Solitons with finite wavelength, *Physical Review Letters*, Vol. 70, No. 5, 1993, pp. 564–567.

[2] J. de Frutos, M. A. López-Marcos and J. M. Sanz-Serna, A finite difference scheme for the $K(2,2)$ compacton equation, *Journal of Computational Physics*, Vol. 120, No. 2, 1995, pp. 248–252.

[3] P. Saucez, A. Vande Wouwer, W. E. Schiesser and P. Zegeling, Method of lines study of nonlinear dispersive waves, *Journal of Computational and Applied Mathematics*, Vol. 168, 2004, pp. 413–423.

[4] A. Chertock and D. Levy, Particle methods for dispersive equations, *Journal of Computational Physics*, Vol. 171, 2001, pp. 708–730.

[5] F. Rus and F. R. Villatoro, Padé numerical method for the Rosenau-Hyman compacton equation, in *Modelling 2005, Third IMACS Conference on Mathematical Modelling and Computational Methods in Applied Sciences and Engineering*, Pilsen, Czech Republic, July 4-8, 2005. Currently under review in *Mathematics and Computers in Simulation.*

[6] D. Levy, C.-W. Shu, J. Yan, Local discontinuous Galerkin methods for nonlinear dispersive equations, *Journal of Computational Physics*, Vol. 196, 2004, pp. 751–772.

[7] M. S. Ismail, T. R. Taha, A numerical study of compactons, *Mathematics and Computers in Simulation*, Vol. 47, 1998, pp. 519–530.

[8] J. M. Sanz-Serna and I. Christie, Petrov-Galerkin methods for nonlinear dispersive waves, *Journal of Computational Physics*, Vol. 39, No. 1, 1981, pp. 94–102.

[9] P. Rosenau, On a class of nonlinear dispersive-dissipative interactions, *Physica D*, Vol. 123, No. 1–4, 1998, pp. 525–546.